The $B(E2;0^+_{gs} \rightarrow 2^+)$ systematics of Sn and Te isotopes in light of data in the light Sn region including a recent measurement in ^{108}Te using the combined recoil–decay–tagging–recoil-distance Doppler technique

2012 Phys. Scr. 2012 014003

(http://iopscience.iop.org/1402-4896/2012/T150/014003)

Phys. Scr. **T150** (2012) 014003 (4pp) doi:10.1088/0031-8949/2012/T150/014003

The $B(E2;0^+_{gs} \rightarrow 2^+)$ systematics of Sn and Te isotopes in light of data in the light Sn region including a recent measurement in ^{108}Te using the combined recoil–decay–tagging–recoil-distance Doppler technique

T Bäck[1], C Qi[1], B Cederwall[1], R Liotta[1], F Ghazi Moradi[1], A Johnson[1], R Wyss[1] and R Wadsworth[2]

[1] Royal Institute of Technology, SE-10691 Stockholm, Sweden
[2] Department of Physics, University of York, York YO10 5DD, UK

E-mail: back@nuclear.kth.se

Received 6 June 2012
Accepted for publication 6 August 2012
Published 28 September 2012
Online at stacks.iop.org/PhysScr/T150/014003

Abstract
An experimental technique combining the well-established α/p–decay–recoil–tagging method with a differential plunger has recently been successful in producing results in the neutron-deficient region near ^{100}Sn. This experimental technique is briefly presented here and the result of a recent measurement for ^{108}Te is put in the context of the systematics of B(E2) values for the Te and Sn isotopic chains. New state-of-the-art shell-model calculations are presented for the Sn data, and possible explanations for the unusually large B(E2) values for the Sn isotopes near the $N = 50$ shell closure are given.

PACS numbers: 21.10.Tg, 21.60.Cs

(Some figures may appear in colour only in the online journal)

1. Introduction

The region near the doubly magic shell closure at ^{100}Sn is very attractive as a testing ground for nuclear models. Here we expect an increase in stability and binding energy as we approach the closed shell at $N = Z = 50$. On the other hand, ^{100}Sn is situated far from the stability line and near the proton drip line. Another aspect of interest in this region is the expected enhancement of neutron–proton interaction due to the fact that the neutrons and protons move in identical orbitals. Many nuclides in the region just above the $N = Z = 50$ shell have an important feature seen from the experimental aspect; they are unstable to α (and/or proton) decay. As explained below, this enables us to use decay-tagging techniques to extract experimental information even from weakly populated reaction channels.

Recently, experiments utilizing Coulomb excitation of light Sn isotopes ($^{106,\,108,\,110,\,112}$Sn) have revealed surprisingly large values for the transition rate to the first excited 2^+ state, i.e. $B(E2;0^+_{gs} \rightarrow 2^+)$ [1–4]. From the generalized seniority scheme [5] we would expect the values to drop more rapidly, compared to the experimental data, as we approach the $N = 50$ shell closure. Large-scale shell-model calculations [1–4] could not reproduce the experimental data in these previous studies. A possible explanation for this conundrum has been discussed in terms of a *weakening* of the $N = Z = 50$ shell closures [4]. Another recent set of lifetime measurements [6] challenges the National Nuclear Data Center (NNDC) data in the Sn midshell and suggests a shallow minimum at $N = 66$.

The element tellurium is situated only two protons above tin in the nuclide chart and we expect the same shell-model orbitals to be relevant for both the $_{50}$Sn and $_{52}$Te isotopic chains between $N = 50$ and 82, i.e. $g_{7/2}$, $d_{5/2}$, $d_{3/2}$, $s_{1/2}$ and

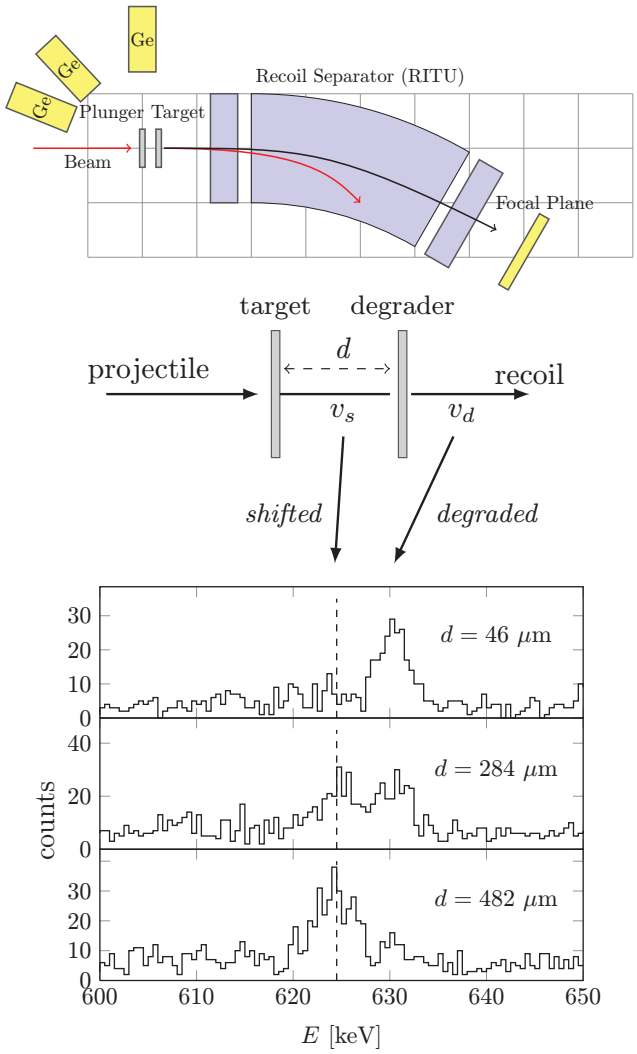

Figure 1. A schematic view of the combined RDT-and-differential-plunger technique at the JYFL facility. The recoils of interest are produced by fusion-evaporation reactions in the target. The movable degrader foil reduces the velocity of the recoils, thereby affecting the angle-dependent Doppler shift of emitted gamma rays. The Ge detectors of the JUROGAM II array are mounted at the angles $\theta = 90^\circ$, $\theta = 134^\circ$ and $\theta = 158^\circ$. Subsequent α-decay events detected (position and E_α) in the focal plane are used to enable a clean selection of the weakly populated reaction channels. The three energy spectra showing the 625 keV peak of ^{108}Te (sample data from [7]) correspond to three target–degrader distances, d. Here, Ge detectors at $\theta = 134^\circ$ were used and the spectra were Doppler corrected for the recoil velocity between the target and the degrader.

$h_{11/2}$. If the shell gap at ^{100}Sn would be reduced we would therefore expect a strong enhancement also of the transition probabilities in the tellurium isotopes as we approach $N = 50$. An addition to the $B(\mathrm{E2}; 0^+_{\mathrm{gs}} \rightarrow 2^+)$ systematics of the Te isotopic chain was recently made with a measurement in ^{108}Te [7]. Before the experiment in [7] no B(E2)-data for tellurium isotopes existed for isotopes lighter than ^{114}Te. The *leap* to ^{108}Te was made possible by combining the recoil–decay–tagging (RDT) technique and a differential plunger.

After a brief presentation of the RDT/plunger experimental technique, the $B(\mathrm{E2}; 0^+_{\mathrm{gs}} \rightarrow 2^+)$ systematics in Te and Sn are discussed together with the results of new state-of-the-art shell-model calculations.

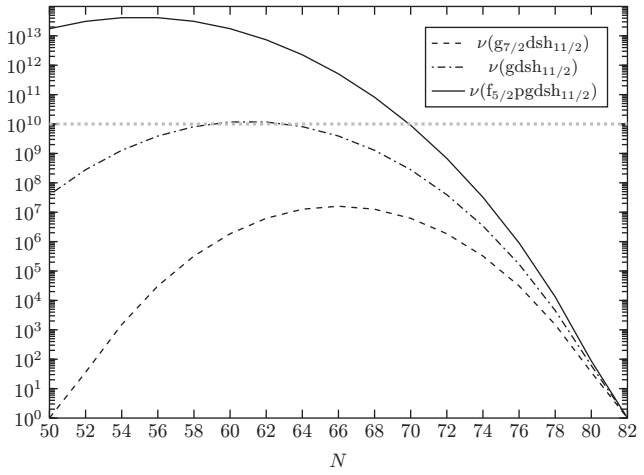

Figure 2. The matrix size in the shell-model calculations presented in this work for three different model spaces. The horizontal line corresponds to our current approximate computing limit for Sn isotopes.

2. The combined RDT–recoil-distance Doppler-shift technique at JYFL, Finland

A combination of the RDT method with the recoil-distance Doppler-shift technique was previously used, e.g., by Grahn *et al* [8] in the neutron-deficient $A = 190$ region. Two experiments measuring transition rates in ^{109}I [9] and ^{108}Te [7] were recently performed at the JYFL accelerator facility in Jyväskylä, Finland, establishing this complex technique in the region just above ^{100}Sn and close to the $N = Z$ line. In both these experiments an ion beam bombarded a production target situated in the centre of the gamma-ray detector array JUROGAM II, consisting of 39 Compton-suppressed germanium detectors from the former Euroball array [10]. The recoils formed by the fusion-evaporation-type reaction in the target were subsequently transported through the gas-filled RITU recoil separator [11] and implanted in the position-sensitive double-sided silicon strip detector of the focal plane detector system GREAT [12]. The unique energy of the charged particle decays (e.g. α-decay for ^{108}Te, proton emission for ^{109}I) could then be used to *tag* the prompt gamma photons (emitted near the production target) belonging to a particular nuclide. An extreme level of selectivity is achieved with this so-called RDT technique. In these experiments, the RDT method was combined with a plunger technique in order to measure picosecond-scale lifetimes of excited nuclear states. For this purpose, the Köln differential plunger [13], mounted in the centre of JUROGAM II, positioned a degrader foil (natural Mg, 1 mg cm^{-2}) at a number of precisely selected distances from the production target. The recoiling nuclei travelled at a constant velocity in the short distance between the production target and the degrader foil, and then at a lower velocity after the degrader foil. The Doppler shift of the gamma rays could then be used to determine the position of decay and the lifetime could be extracted after measurements at a number of target–degrader distances. In the off-line analysis, the lifetime, τ, of e.g. the excited 2^+ state in ^{108}Te was extracted using the well-established differential decay curve method [14]. Gamma detectors in JUROGAM II at angles $\theta = 134^\circ$ and 158° could be used to extract the intensity of

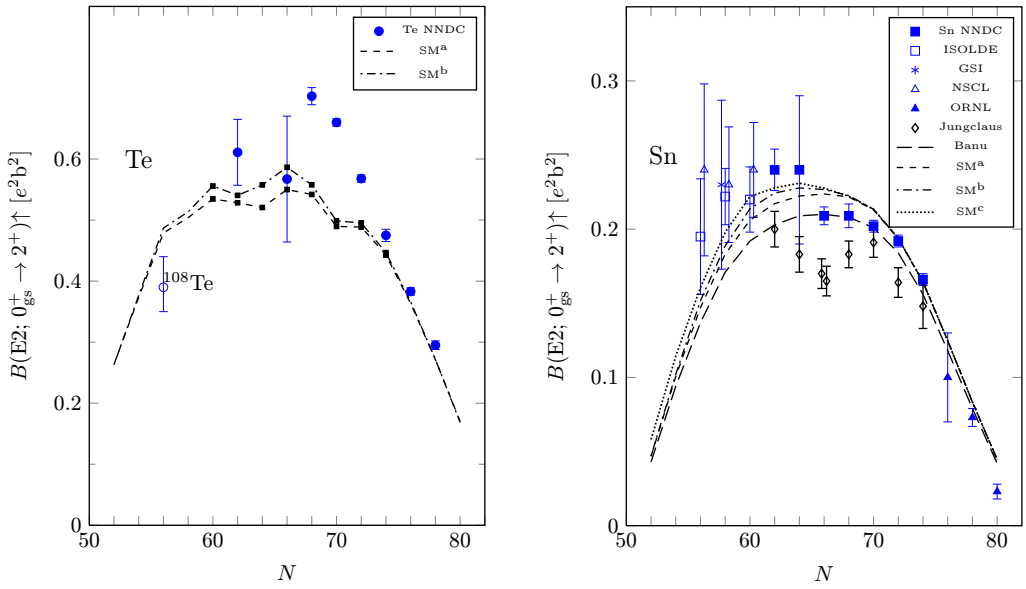

Figure 3. Left panel: experimental ($0^+_{gs} \rightarrow 2^+$) transition rates for Te isotopes (http://www.nndc.bnl.gov/be2/) with the new data point [7] added at ^{108}Te (open circle). Shell-model curves in the model space ($g_{7/2}$, d, s, $h_{11/2}$), using the effective charges: $e^{\nu}_{\rm eff} = 0.8e$, $e^{\pi}_{\rm eff} = 1.5e$, reproduce the general trend of the Te data. The underestimation of the values in the midshell is related to a limitation in the calculation of the midshell tellurium isotopes (marked by small solid squares) allowing only four particles above the Fermi level to be excited into the $h_{11/2}$ orbital. This limitation generates the unsmooth behaviour of the calculated Te values in the midshell. The dashed curve (SM^a) corresponds to single-particle energies according to [1]. For the dash-dotted curve (SM^b) the $d_{5/2}$, $g_{7/2}$ orbitals were inverted. Right panel: experimental $B(E2; 0^+_{gs} \rightarrow 2^+)$ data for Sn isotopes from [1–4, 6, 17] compared to several sets of shell-model calculations: SM^a and SM^b use the same model space and ε_{sp} as for tellurium. For SM^c, the neutron $g_{9/2}$ orbital is added to the model space. The values of Banu *et al* [1] using a constant oscillator energy $\hbar\omega = 8.5$ MeV is used for comparison. For Sn, the SM^{a-c} use $e^{\nu}_{\rm eff} = 1.0e$ as in [1].

the shifted (I_s) and degraded (I_d) components for several different target–degrader distances, see figure 1. The quantity $Q = I_d/(I_s + I_d)$ was then calculated as a function of the plunger distance for the low-lying transitions in ^{109}I and ^{108}Te. The lifetimes of the states were extracted using the values of Q and its derivative for transitions feeding and depopulating the states of interest at different target–degrader distances, using the method in [14]. For ^{108}Te this analysis gave a measured lifetime for the 2^+ state of $\tau = 11.0 \pm 1.3$ ps. This corresponds to a $B(E2; 0^+_{gs} \rightarrow 2^+)$ value of $0.39^{+0.05}_{-0.04} e^2b^2$. For more details of this specific experiment and its data analysis, see [7].

3. Discussion

It is well known that the nuclear shell model is successful in predicting nuclear properties near closed shells. On the other hand, our picture of shell structure far from stability, e.g. in the ^{100}Sn region, is far from complete. In order to investigate the ability of modern shell-model theory to predict $B(E2; 0^+_{gs} \rightarrow 2^+)$ values in the region just above the $N, Z = 50$ shell closure, recent experimental data (including the data point at ^{108}Te from [7]) were compared with new shell-model calculations covering the systematics from $N = 50$ to 82 for Te and Sn isotopes. These calculations use the CD-Bonn interaction [15], renormalized by using the perturbation approach according to [16]. In all the calculations presented here, we have used a constant 6 MeV shell-gap energy at $N = Z = 50$.

The Sn/Te region lies at the very edge of capability of modern shell-model calculations. The dimension of the problem grows beyond even the modern computer systems for the shell-model spaces that we need to consider. As an example, the full proton/neutron g, d, s, $h_{11/2}$ space, e.g. including $g_{9/2}$ core excitations for both neutrons and protons, gives a matrix dimension of 10^{18}, well beyond our current capability of around 10^{10}. In figure 2 we show the problem matrix dimension as a function of the neutron number for three different neutron model spaces.

The $B(E2; 0^+_{gs} \rightarrow 2^+)$ data of the Te and Sn isotopic chains are presented in figure 3. The first thing one notes in this figure is that the $B(E2)$ values for Te lies 2–3 times higher than the Sn data. This can be understood in terms of the additional neutron–proton interaction generated by the two extra protons present in Te above the $Z = 50$ shell closure. For tellurium, the data point at ^{108}Te suggests an almost symmetric trend in the experimental data with respect to the neutron midshell. The shell-model curve (model space: $g_{7/2}$, $d_{5/2}$, $d_{3/2}$, $s_{1/2}$, $h_{11/2}$) agrees rather well with the data. The model underestimates the data in the midshell where the calculation had to be limited by allowing only up to four particles above the Fermi level for the $h_{11/2}$ orbital. The shell-model calculation for Te shown here is identical to that presented in [7].

For the $B(E2; 0^+_{gs} \rightarrow 2^+)$ systematics of Sn isotopes, see figure 3, the unusually large experimental values at $^{106-110}$Sn lie approximately 30% above the previous shell-model predictions [1]. In this way, an *asymmetry* with respect to the neutron midshell is clearly present in the data, but is not reproduced by the model curves, see [1–4], and a possible weakening of the $N = Z = 50$ shell closures [4] has been discussed.

In our new calculations, we investigate possible origins of the asymmetry, within the framework of the shell model and without reducing the $N = Z = 50$ gap energy. First we note that using an N-dependent oscillator ($\hbar\omega$) energy in the calculation changes the curve, and gives a slight asymmetry. This is a standard procedure, but in [1], which we use as a reference curve in figure 3, a constant value ($\hbar\omega = 8.5$ MeV) was used. We first tested the effect of inverting the $d_{5/2}$, $g_{7/2}$ orbitals, separated by 172 keV, but for which the order is still debated [18–20]. The inversion is mainly motivated by the recent experimental results of Darby *et al* [18]. It is clear from figure 3 that this inversion of orbitals mainly affects the midshell of the Te isotopes, but that it generates a clear (although modest) asymmetry in the model curve for Sn. A third contribution to the asymmetry we found when including the $g_{9/2}$ neutron orbital in the calculation, see the SM^c curve in figure 3. We interpret the enhancement of transition rates as a Pauli blocking effect related to the core excitations from the $g_{9/2}$. This Pauli blocking becomes more important as we fill the neutron shells above the $N = 50$ shell gap, and the enhancement of the B(E2) values is therefore lost as we approach the neutron midshell. As pointed out in [7], we expect this Pauli blocking effect to be less important for Te, seen relative to the much larger absolute transition probabilities in Te. It should be noted that including the $g_{9/2}$ *proton* did not in itself give any asymmetry in the B(E2) curve for Sn, in agreement with the results of [1–4].

As mentioned above, the new data of Jungclaus *et al* [6] are in contrast to the adopted NNDC values in the Sn midshell, see figure 3. More independent experimental results are needed to understand this anomaly. We note that in our calculation the shape of the model curve in the midshell is quite sensitive to the exact energies of the $d_{3/2}$, $s_{1/2}$ and $h_{11/2}$ single-particle orbitals.

4. Summary

To summarize, the technique of combining RDT with the recoil-distance Doppler method has recently been established in the region just above ^{100}Sn in the nuclide chart by experiments at the JYFL facility in Jyväskylä, Finland. Recent results include lifetime data in ^{108}Te [7] and ^{109}I [9]. The $B(\mathrm{E2}; 0^+_{gs} \rightarrow 2^+)$ value in ^{108}Te agrees rather well with the results of our large-scale shell-model calculations using the CD-Bonn potential. Our new calculations investigate the systematics of $B(\mathrm{E2}; 0^+_{gs} \rightarrow 2^+)$ values for tin isotopes. The result suggests that the asymmetry with respect to the neutron midshell seen in the data could be related to both the order of the $d_{5/2}$ and $g_{7/2}$ single-particle orbitals as well as to the Pauli blocking of neutron core excitations.

References

[1] Banu A *et al* 2005 *Phys. Rev.* C **72** 061305
[2] Cederkäll J *et al* 2007 *Phys. Rev. Lett.* **98** 172501
[3] Vaman C *et al* 2007 *Phys. Rev. Lett.* **99** 162501
[4] Ekström A *et al* 2008 *Phys. Rev. Lett.* **101** 012502
[5] Talmi I 1971 *Nucl. Phys.* A **172** 1
[6] Jungclaus A *et al* 2011 *Phys. Lett.* B **695** 110
[7] Bäck T *et al* 2011 *Phys. Rev.* C **84** 041306
[8] Grahn T *et al* 2009 *Eur. Phys. J.* A **39** 291
[9] Procter M *et al* 2011 *Phys. Lett.* B **704** 118
[10] Beck F 1992 *Prog. Part. Nucl. Phys.* **28** 443
[11] Leino M *et al* 1995 *Nucl. Instrum. Methods* B **99** 653
[12] Page R *et al* 2003 *Nucl. Instrum. Methods* B **204** 634
[13] Fransen C *et al* 2010 *J. Phys: Conf. Ser.* **205** 012043
[14] Dewald A *et al* 1989 *Z. Phys.* A **334** 163
[15] Machleidt R 2001 *Phys. Rev.* C **63** 024001
[16] Hjorth-Jensen M *et al* 1995 *Phys. Rep.* **261** 125
[17] Radford D *et al* 2004 *Nucl. Phys.* A **746** 83c
[18] Darby I *et al* 2010 *Phys. Rev. Lett.* **105** 162502
[19] Seweryniak D *et al* 2007 *Phys. Rev. Lett.* **99** 022504
[20] Ressler J *et al* 2002 *Phys. Rev.* C **65** 044330